Hydration of potassium citrate-activated BOF slag

Cement and Concrete Research 140 (2021) 106291

Contents lists available at ScienceDirect

Cement and Concrete Research

journal homepage: www.elsevier.com/locate/cemconres

Hydration of potassium citrate-activated BOF slag

A.M. Kaja [a], K. Schollbach [a,b], S. Melzer [b], S.R. van der Laan [a,b], H.J.H. Brouwers [a], Qingliang Yu [a,c,*]

[a] Department of the Built Environment, Eindhoven University of Technology, Eindhoven 5600 MB, the Netherlands
[b] Tata Steel, R&D, Microstructure & Surface Characterization (MSC), P.O. Box 10.000, 1970 CA, IJmuiden, the Netherlands
[c] School of Civil Engineering, Wuhan University, 430072 Wuhan, PR China

ARTICLE INFO

Keywords:
BOF slag
Brownmillerite
Chemical activation
Tri-potassium citrate
Microstructure

ABSTRACT

Basic Oxygen Furnace (BOF) slag is currently utilized with low-grade applications or landfilled. Here, we investigate a novel route to upgrade BOF slag to a high-performance binder by chemical activation with tri-potassium citrate. The impact of tri-potassium citrate on hydration and phase assemblage of BOF slag is analyzed with a multi-technique approach. Results reveal that the addition of tri-potassium citrate considerably enhances the reactivity of brownmillerite and accelerates the hydration of belite at early ages. The majority of brownmillerite hydrates within 24 h, and the reaction kinetics is controlled by the activator dosage. The main products of BOF slag hydration are siliceous hydrogarnet and C-S-H gel. Acting as a strong water reducer, tri-potassium citrate enables the manufacture of slag pastes with high compressive strength (up to 75 MPa at 28 days) and low porosity. Leaching of heavy metals from the slag pastes fulfills the Dutch Soil Quality Decree limits.

1. Introduction

Basic Oxygen Furnace (BOF) slag is a by-product of the conversion of iron to steel during the Linz-Donawitz process, and therefore, also called LD slag or converter slag [1]. Around 90–110 kg of BOF slag are generated per ton of steel produced, resulting in the annual production of BOF slag of about 10.4 million tons in Europe [2–5]. The BOF slag is composed of CaO (30–50%), SiO_2 (10–20%), Fe_2O_3 (20–40%), Al_2O_3 (1–7%), MgO (4–10%), MnO (0–4%), P_2O_5 (1–3%) and TiO_2 (0–2%) [6], with a mineral assemblage of C_2S, C_3S, $C_2(A,F)$, RO phase (CaO–FeO–MgO–MnO solid solution, crystallized in wuestite structure), and free lime (CaO) [2,7,8]. Despite the presence of C_2S/C_3S and $C_2(A,F)$ phases, the hydraulic activity of the slag tends to be rather low, which hinders its application as a binder constituent [9]. The utilization of BOF slag in concrete is further limited due to the volume instability problems caused by the presence of free CaO [10] and the contamination with heavy metals [11] (especially vanadium and chromium [2,12]).

Since C_3S is only a minor component of BOF slag (typically 0–5 wt%) [2], up to now, researchers have been mainly focusing on the activation and hydration of C_2S- the most abundant phase in the BOF slag (40–55 wt%) [13]. The C_2S phase (belite) appears in BOF slag as α' and β polymorphs. Without any treatment (physical or chemical), the early age hydraulic activity of belite is very low. The activation of BOF slag with conventional alkaline activators (like NaOH) as well as other admixtures, including $CaCl_2$, NaCl, Na_2SiO_3, high alumina cement, and commercial accelerator has been shown to only slightly affect the hydration of BOF slag [13,14]. One possible reason is the stabilization of belite in the presence of impurities (Fe^{3+}, P^{5+}) [10,15]. The impurities tend to decrease the reactivity of C_2S, and this effect is particularly visible with the high concentration of the contaminants [16].

Contrary to belite, limited attention has been paid to the second most abundant hydraulic phase in BOF slag –brownmillerite, also called srebrodolskite (~20 wt%). Whereas the hydration of belite in Portland cements contributes mainly to the late strength development (beyond 28 days), the dissolution and hydration of brownmillerite occur simultaneously with tricalcium aluminate, leading to the rapid formation of the products such as Fe-containing AFm phases and hydrogarnets [17,18]. The extent of brownmillerite reaction is, however, significantly lower than that observed for C_3A [19]. In cement, the composition of the brownmillerite can be close to C_6A_2F but in general, tends towards C_6AF_2 or even C_2F [20]. With an increased iron content, the reactivity of brownmillerite decreases [21]. In consequence, the hydraulic activity of brownmillerite in Fe-abundant and Al-deficient BOF slags is expected to be low. Schwarz [22] postulated that the dissolution of brownmillerite

* Corresponding author at: Department of the Built Environment, Eindhoven University of Technology, Eindhoven 5600 MB, the Netherlands.
E-mail address: q.yu@bwk.tue.nl (Q. Yu).

https://doi.org/10.1016/j.cemconres.2020.106291
Received 15 May 2020; Received in revised form 30 October 2020; Accepted 5 November 2020

can be enhanced with the addition of citrate salts – where citrate is assumed to act via surface complexation and ligand-promoted dissolution. The formation of stable citrate complexes with iron has also been reported previously [23]. However, in the study of Möschner et al. [24], while using citric acid (up to 0.5 wt%), no experimental evidence for this phenomenon was observed. Instead, the sorption of the citrate species on the clinker surface was suggested. Nevertheless, the effect of potassium citrate- a basic salt, compared to the citric acid, can differ substantially, since the behavior of citrate species, as well as the dissolution rate of cementitious phases, strongly depend on the pH [25,26].

In this study, we report a novel, Portland cement-free, high-performance binder made from BOF slag and tri-potassium citrate monohydrate that plays a dual role of superplasticizer and activator of iron-containing phases. The influence of the tri-potassium citrate dosage on the phase development, microstructural and mechanical properties of BOF slag pastes is investigated using a multi-technique approach, based on quantitative XRD analysis, in-situ XRD, SEM/EDX large area phase mapping combined with PhAse Recognition and Characterization (PARC) software, thermogravimetric analysis, calorimetric measurements, porosimetry (MIP) and mechanical performance testing. In addition, leaching tests are performed on the final products in order to evaluate the environmental impact and consequently, the potential for the utilization of BOF slag in the concrete industry.

2. Materials and methods

2.1. Materials and mix design

A representative mixture of BOF slag, collected from standard production, provided by Tata Steel (The Netherlands), was used in this study. Before the application, slag was ground using a planetary ball mill (Pulverisette 5, Fritsch) and sieved below 106 μm. Fig. 1 shows the particle size distribution of BOF slag after mechanical treatment as measured by laser diffraction spectroscopy (Mastersizer 2000, Malvern).

The chemical and mineralogical compositions of BOF slag were determined with XRF analysis and XRD Rietveld method and are presented in Table 1. The additive, tri-potassium citrate monohydrate ($K_3C_6H_5O_7{\cdot}H_2O$), was a commercially available technical grade product (GPR RECTAPUR®, purity >99%).

BOF slag pastes containing tri-potassium citrate monohydrate were prepared with the water/binder ratio (w/b) of 0.16 to avoid bleeding and segregation (an exception was made for the reference sample with the w/b ratio of 0.24). In the reference sample, the w/b was chosen based on preliminary experiments in order to minimize the differences in the initial water content between the reference and activated samples, and at the same time to enable sufficient workability for mixing and

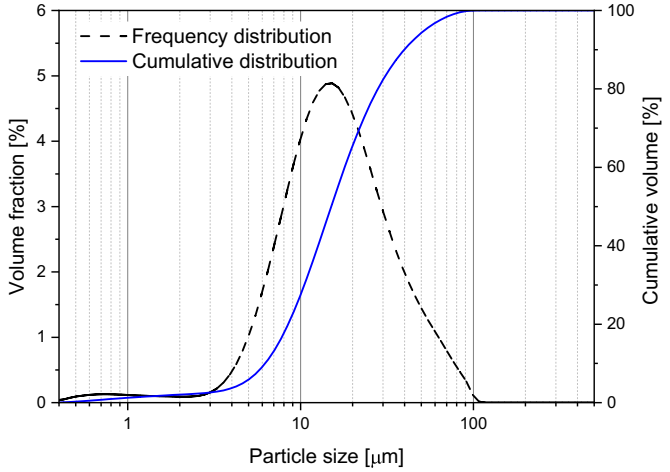

Fig. 1. The particle size distribution of BOF slag.

Table 1
Mineralogical and chemical composition of BOF slag.

Mineral compound	Content [wt%]	Oxide	Content [wt%]
Brownmillerite	17.4	MgO	8.04
Magnetite	10.9	SiO_2	13.8
C_2S	31.6	Al_2O_3	2.44
Wuestite	21.1	CaO	39.5
Lime	0.5	P_2O_5	1.67
Calcite	0.6	TiO_2	1.45
Portlandite	1.2	V_2O_5	1.05
C_3S	0.2	Cr_2O_3	0.3
Amorphous	16.5	MnO	4.4
		Fe_2O_3	29.0
		SrO	0.02
		Na_2O	<0.2
		K_2O	<0.01
		GOI 1000	1.41

casting of the paste. Prior to the mixing, three different concentrations of potassium citrate, equivalent to 1, 2, and 3 wt% of slag were added to the water to ensure a homogenous dispersion. The pastes were mixed for 3 min with a high-speed mixer. Subsequently, they were stored at 20 °C in plastic vials sealed with parafilm in a desiccator filled with water and sodium hydroxide pellets in order to minimize carbonation. The samples are named based on the amount of K_3-citrate added: C0, C1, C2, C3 for 0, 1, 2, 3% (by mass of slag) of K_3-citrate dosage, respectively.

2.2. Methodology

The isothermal conduction calorimeter (TAM Air, Thermometric) was used to determine the rate of heat release during the first 7 days of hydration. Powders were externally mixed with tri-potassium citrate solutions for 1 min to ensure a homogenous paste. In order to evaluate the cumulative heat, the heat flow curve was integrated between 45 min and 200 h.

Scanning electron microscopy (SEM) measurements combined with energy-dispersive X-ray spectroscopy (EDX) analyses were performed on the pastes after 28 days of hydration. Before the measurements, pastes were cut with a saw to 2–3 mm slices, gently broken into smaller pieces, then immersed in isopropanol for 3 days and vacuum dried. The small pieces were subsequently embedded in epoxy resin, polished and coated with carbon for SEM analyses. The spectral imaging (SI) data were acquired with a JEOL JSM-7001F SEM equipped with two 30 mm^2 SDD detectors (Thermo Fisher Scientific) and a NORAN-System7 with NSS.3.3 software. A beam current in the focused probe of 6.2 nA and an accelerating voltage of 15 kV were used. The step size was 1 μm, with an individual SI field comprising of 512 × 384 pixels. For each sample, 16 fields were analyzed.

The PhAse Recognition and Characterization (PARC) software was used to determine the chemical composition of the original slag phases and the hydration products as well as to quantify the phase composition of unhydrated, unmilled BOF slag. Detailed information about the PARC technique is provided elsewhere [27]. The data acquired with EDX mapping were processed with the PARC software by grouping each data point by its chemical composition into phases. Therefore, in contrast to the XRD Rietveld method, PARC software enabled the quantification of different phases, including amorphous ones (note the resolution of 1 μm). In order to acquire a representative chemical composition of the BOF slag phases and hydration products, an erosion filter was applied to exclude the data from the boundaries of phases. After erosion, only pixels surrounded by eight neighboring pixels allocated to the same phase were used for analysis. The quantitative phase analysis of BOF slag was performed on unmilled material (with the particle size between 1 and 2 mm) in order to minimize the error caused by the analysis of very fine particles. The densities of the converter slag phases used for the calculations of phase mass were derived from the Rietveld refinement.

For the quantitative XRD analysis, slag pastes were crushed in an

agate mortar, and hydration was stopped with the double solvent exchange method (15 min in isopropanol, flushing with diethyl ether, 8 min drying at 40 °C in a half vacuum condition). The powders were milled with an XRD-Mill McCrone (RETSCH) and backloaded into sample holders. Corundum was used as an external standard [28]. The diffraction patterns were collected with a D4 ENDEAVOR X-ray Diffractometer equipped with a LynxEye detector and Co X-ray tube. Samples were measured on a rotating stage (with a rotation speed of 30 rpm) using a step size of 0.014° 2θ and a time per step of 1 s for a 2θ range of 12–80° 2θ. The data analyses were performed with TOPAS Academic software v5.0. The ICSD codes for the crystal structures used during the Rietveld refinement are provided in Table 2. In order to account for the high magnesium and manganese content in wuestite, as well as the low aluminum content and the presence of titanium in brownmillerite, the structural data sets for these phases were corrected based on the ion substitution levels derived from the PARC analyses. To calculate the absolute amounts of the phases, the G-factor method was applied [28,29]. The lattice and microstrain parameters were refined in the anhydrous slag and then used for the refinement of the pastes.

In-situ XRD test was performed with an X'Pert Pro PANalytical diffractometer equipped with a position-sensitive X'Celerator detector and Co X-ray tube, using an β-filter (iron foil). After 2 min of mixing with a high-speed mixer, the sample was inserted into the sample holder and covered with Kapton foil to minimize water evaporation and carbonation. The temperature of the sample was measured with a custom-made sample holder mounted on an Anton-Paar HTK2000 heating stage. Each diffractogram was recorded for 15 min in the range between 10 and 80° 2θ with a step size of 0.02 2θ, for up to 50 h of hydration.

The thermal behavior of the powdered samples (40–60 mg) was analyzed using a Jupiter STA 449 F1 Netzsch instrument. The samples were heated up to 1000 °C at the rate of 5 °C/min under a nitrogen atmosphere. The amount of portlandite was quantified with a tangential method. The bound water content was determined based on the mass loss between 40 °C and 500 °C.

The FT-IR spectra of slag pastes were collected using a PerkinElmer Frontier™ MIR/FIR Spectrometer with the attenuated total reflection (ATR) method (GladiATR). All spectra were scanned 24 times from 2000 to 600 cm^{-1} at a resolution of 2 cm^{-1}.

In order to observe the morphology of the hydration products, the FEI quanta 600 environmental scanning electron microscope was used to perform the SEM analyses on the 28 days hydrated pastes. Before analyses, the samples were sputtered with gold by using an Emitech K550X sputter coater (current 65 mA, coating time 20 s). Micrographs were recorded with the secondary electron detector at 5 kV at 65000× magnification.

For Mercury Intrusion Porosimetry (MIP) measurements, after 28 days of hydration, the samples were cut into 3 mm cubic pieces, immersed in isopropanol for 7 days and subsequently dried in a desiccator for another 7 days. The AutoPore IV 9500 Micromeritics Series Mercury Porosimeter, with the maximum pressure of 228 MPa, was used for the measurements. The surface tension of mercury (γ_{Hg}) of 485 mN/m and a contact angle (θ) of 130° were adopted for the results interpretation [30].

The compressive strength of the pastes was determined on cubic samples (4 × 4 × 4 cm^3). Pastes were covered with foil and cured in the climate chamber (20 °C, RH > 95%) until the testing age. The 7 and 28 days compressive strengths were determined according to EN 196–1, in three replicates for each composition.

The leaching test was performed on unreacted BOF slag, and 28-days cured slag pastes according to EN 12457–2 (one stage batch leaching test). Hydrated samples were crushed and sieved below 4 mm, the unreacted slag (2-4 mm) was used as is. The experiments were performed with liquid to solid ratios (L/S) of 10 using a dynamic shaker (ES SM-30, Edmund Buhler GmbH) at a constant speed of 250 rpm during 24 h. Ultra-pure water (0.055 uS/cm) was used as a leachant. After 24 h shaking, leachates were filtered through a syringe filter (pore diameter 0.22 μm, Whatman) and acidified with concentrated HNO_3. The solutions were analyzed with an inductively coupled plasma atomic emission spectrometer (ICP-OES, SPECTROBLUE), according to NEN 6966 (NEN-EN 6966, 2005). The obtained elements concentrations were compared with the limit values specified in the Dutch Soil Quality Decree [31].

Table 2
Structural data of the phases used for the Rietveld refinement.

Phase	ICSD
Brownmillerite	9197*
α'-C_2S	81,097
Wuestite	67200*
C_3S	64,759
β-C_2S	245,074
Magnetite	20,596
Lime	28,905
Portlandite	202,220
Hydroandradite	29247*
Katoite	9272
Pyroaurite	6295

* The structures were modified based on the PARC analyses.

3. Results and discussion

3.1. Characterization of unhydrated BOF slag

The surface exposure of potentially reactive phases of the milled, unreacted slag was evaluated with the PhAse Recognition and Characterization (PARC) analysis. The results are presented in Fig. 2. The phase map generated with the PARC software from SI spectra shows that even though the slag was milled and sieved (below 106 μm), a part of belite and brownmillerite phases is trapped within bigger particles, limiting their accessibility for the reaction.

In order to reveal the chemical composition of the amorphous slag phase, a comparison between the quantitative results of Rietveld and PARC analysis was made. In contrast to XRD Rietveld, the PARC method enables analysis of the amorphous phase and its association with the crystalline counterpart (as the phase determination is based only on the chemical composition). A comparison of the amounts of the phases determined with PARC and XRD Rietveld (as shown in Table 3) indicated that part of the C_2S phase is X-ray amorphous.

By grouping the EDX data points with similar chemical composition into the phases, a sum spectra can be created that gives the average chemical composition of each phase (Table 4). In this way, the presence of minor elements in the phases can also be identified, which is particularly useful for revealing which phases contain heavy metals. The data provided in Table 4 indicate that chromium is mainly located in belite, and vanadium in belite and brownmillerite. It must be noted, however, that the contents of heavy metals derived from the PARC method are overestimated in comparison to XRF analysis.

3.2. Isothermal calorimetry

The isothermal conduction calorimetry results from the reference paste (w/b of 0.24) and pastes containing tri-potassium citrate (w/b of 0.16) are shown in Fig. 3. In the absence of potassium citrate, no distinctive peak is observed which could be assigned to the reaction of slag phases. The heat is evolved mainly within the first 1–2 h and most likely corresponds to the dissolution and to a small extent, the reaction of the dissolving phases (as the heat evolved in this period is higher than that observed in the presence of activator, where the main reaction occurs later). The addition of citrate leads to a distinct heat flow peak, which appears at ~13 h with 1 wt% potassium citrate added. Further increase of potassium citrate dosage results in the shortening of the

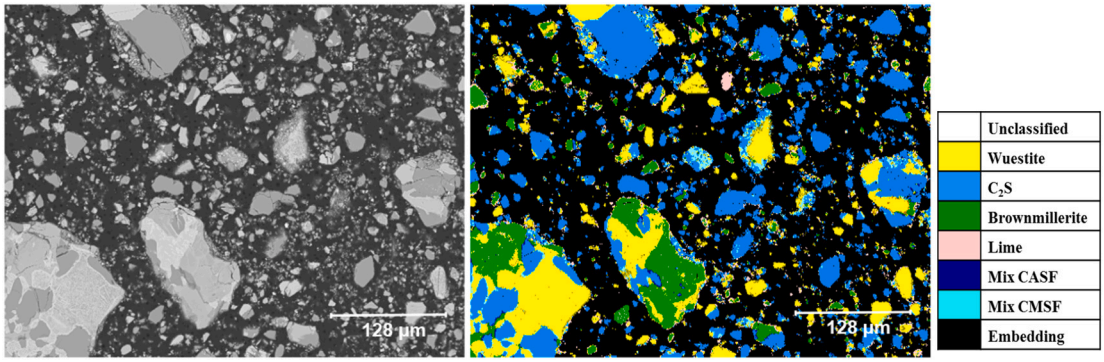

Fig. 2. SEM image of BOF slag after milling (on the left) and corresponding color phase map (on the right) generated with PARC software based on the EDX data. Mix phases are the result of overlapping chemical information from two neighboring phases (where, C, A, M, S, F correspond to CaO, Al_2O_3, MgO, SiO_2 and Fe_2O_3/FeO, respectively).

Table 3
The comparison between the mineralogical composition of BOF slag acquired with Rietveld refinement and PARC analysis.

Mineral compound	PARC	St dev	Rietveld	St dev
Wuestite/magnetite*	30.6	*4.4*	32.0	*1.1*
C_2S	45.7	*5.2*	31.8	*1.9*
Srebrodolskite	14.8	*2.4*	17.4	*0.9*
Lime/portlandite/calcite*	1.1	*0.6*	2.3	*0.2*
Mix phases	5.8	*0.8*		
Amorphous			16.5	*4.5*

* Since with the PARC method, it is not possible to differentiate between lime, portlandite, and calcite as well as between wuestite and magnetite, these phases are grouped together.

induction period and the peak of the heat release rate occurs at approximately 8.5 h and 7.5 h, in the case of 2 wt% and 3 wt% of potassium citrate, respectively. With the increasing amount of potassium citrate, the total heat released after 200 h of hydration increases significantly from 56 J/g_{binder} in the case of the reference sample to 120 J/g_{binder} when 3 wt% of potassium citrate is added.

Even though tri-potassium citrate is usually used as a retarder of the cement/supplementary cementitious materials hydration, its role can differ depending on the applied dosage and w/b ratio. Pacanovsky et al. [32] described that in the systems based on Portland cement and silica fume, tri-potassium citrate salts demonstrate reverse role beyond a certain dosage, switching from retarders to accelerators. Moreover, the required dosage of potassium citrate to become an accelerator decreases with a decreasing w/b ratio. In the slag system, an analogous tendency is observed. In contrast to the reference, the hydration of potassium citrate activated samples is preceded by an induction period. In the same time, with increasing the tri-potassium citrate dosage between 1 and 3 wt%, hydration of BOF slag is accelerated, which is likely to occur with relatively high amounts of tri-potassium citrate used in this study and low w/b ratio.

Table 4
Chemical composition of the main BOF slag phases.

Oxide / Phase	Na_2O	MgO	Al_2O_3	SiO_2	P_2O_5	SO_3	K_2O	CaO	TiO_2	V_2O_5	Cr_2O_3	MnO	Fe_2O_3
Wuestite/magnetite	0.00	23.66	0.20	0.75	0.02	0.00	0.04	2.54	0.03	0.12	0.47	11.71	60.43
Brownmillerite	0.04	0.65	11.22	1.81	0.07	0.01	0.08	42.31	5.14	**1.51**	0.38	1.26	35.01
C_2S	0.15	0.28	0.54	28.19	3.38	0.15	0.11	61.41	1.19	**1.11**	**1.22***	0.09	2.17

* The Cr_2O_3 analysis should be treated with caution since the Cr emission spectrum overlaps with the sum peak of Ca + Si Kα.

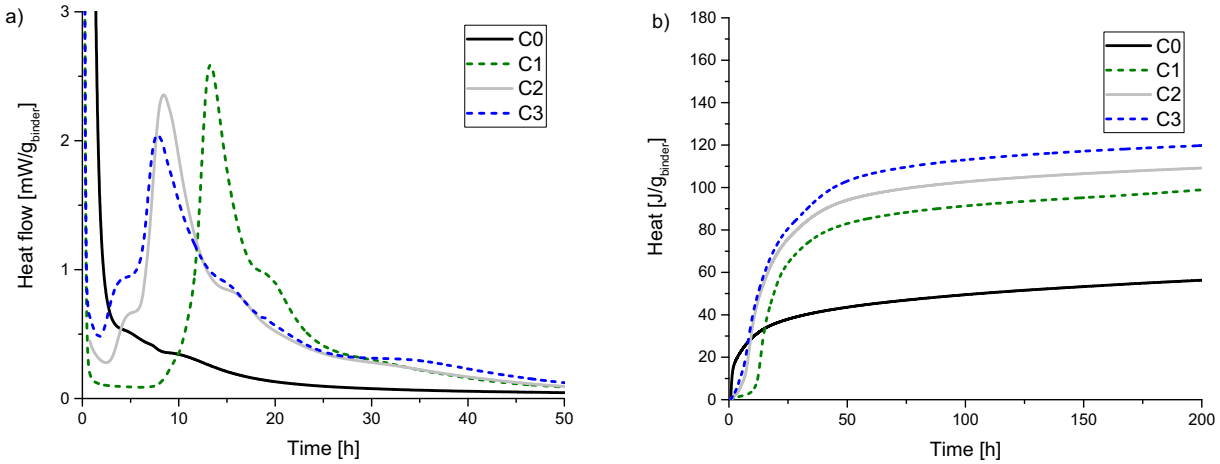

Fig. 3. Heat flow and cumulative heat evolution of slag pastes with dosages of tri-potassium citrate varying from 0 to 3 wt%.

3.3. Identification of reactive phases

In order to evaluate which reactive phases contribute to the heat release observed with the isothermal calorimetry, the early age hydration was monitored with in-situ XRD. Fig. 4 shows the XRD patterns recorded within the first 50 h of hydration of the paste with 3 wt% of tri-potassium citrate. An apparent decrease in the peak intensity at 39° 2θ can be observed, showing that brownmillerite is the most reactive phase at the early hydration age.

The hydration of brownmillerite and other BOF slag phases was further investigated with ex-situ experiments and subsequent quantification using the XRD Rietveld method. The reference sample and the tri-potassium citrate activated samples were analyzed after 7 and 28 days of hydration and compared with the unreacted BOF slag (Table 5). From the XRD Rietveld analyses, it appears that hydration of brownmillerite occurs mainly up to 7 days, and its extent is highly influenced by the activator dosage. In the sample with the highest activator dosage (3 wt %), almost 70 wt% of brownmillerite undergoes reaction. Rapid hydration of brownmillerite observed with in-situ and ex-situ XRD methods corresponds well with the heat evolvement detected with the isothermal calorimetry.

The extent of belite hydration is also affected by the presence of the activator. After 7 days of hydration, a decrease of belite content with increasing amount of added activator is observed. This effect is likely due to the higher alkalinity of the pore fluid in the presence of tri-potassium citrate. The accelerated reaction of C_2S at the early hydration ages was previously reported with conventional alkaline activation [14]. After 28 days of hydration, however, the belite content is similar in all samples, with a tendency towards a higher degree of reaction in the series with 1 wt% of potassium citrate.

Next to the brownmillerite and belite, during the investigated period, the dissolution of wuestite also takes place. Analogously to the belite phase, wuestite exhibits increased early age reactivity in the presence of activator. Previous studies implied that the reactivity of wuestite is related to its chemical composition, especially the magnesium content [33]. In general, the higher the magnesium content, the greater the extent of wuestite dissolution is reported [34]. Moreover, it was revealed by De Windt et al. [12], by investigating the leaching properties, that the degree of wuestitie dissolution depends on particle size distribution, degree of surface alteration and water to solid ratio applied (associated with the pH variation). With lower water to solid ratios, higher leaching of elements was reported. It is therefore likely that the observed reactivity of wuestite phase is mainly a result of surface alterations caused by the applied milling procedure, low w/b ratios as well as favorable chemical composition. It must be noted, that the reactivity of wuestite observed with the XRD analysis might be slightly overestimated due to the sample preparation procedure, where the milling time must be balanced to ensure sufficient grinding of hard phases (e.g. wuestite) and to prevent the hydration products from amorphization. In contrast, the magnetite content is relatively stable in all pastes at the investigated hydration ages.

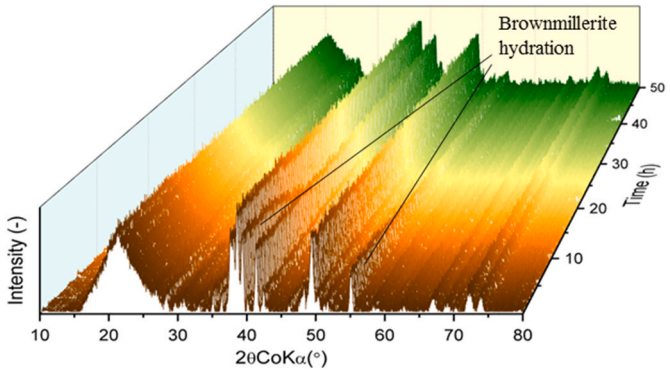

Fig. 4. In-situ XRD patterns of the hydrating slag with 3 wt% of activator dosage, within 50 h of hydration. The peak in the range between 15 and 30° 2θ is due to the Kapton foil and free water.

3.4. Hydrates assemblage

The XRD analyses revealed the presence of three crystalline hydration products: siliceous hydrogarnet, pyroaurite, and portlandite (Fig. 5). Formation of siliceous hydrogarnets, with the general chemical formula $Ca_3(Al_xFe_{1-x})_2(SiO_4)_y(OH)_{4(3-y)}$, was previously observed for Portland cement systems [17,35–37]. Among iron-rich hydration products, reported in the literature (including hydrogarnets, ferrihydrites, Fe-containing AFm and Fe-ettringite), hydrogarnets are the most stable iron-containing phases [18].

Since in the structure of hydrogarnet Fe^{3+} can be substituted by Al^{3+} in octahedral positions and SiO_4^{4-} by $4OH^-$ in tetrahedral positions, the determination of the chemical composition of hydrogarnets becomes difficult, especially at the early hydration ages when metastable phases such as silica-free hydrogarnets (Fe-katoite) can form [18,38]. Dilnesa et al. [18] suggested the occurrence of solid solution between hydrogarnets with low and high silica content as well as between iron and aluminum containing end members. The occurrence of hydrogarnets with varying chemical composition results in the broadening of XRD reflections (see Fig. 5). In order to provide the best possible quantification of this phase, in the Rietveld analysis, two structures, including low-silica hydrogarnet (Fe-katoite, ICSD: 9272) and high-silica hydrogarnet (hydroandradite, ICSD: 29247) were adopted. Additionally, the structure of hydroandradite was adjusted for the iron substitution with aluminum, based on the PARC analysis, assuming that hydroandradite contains most of the available iron and aluminum. The following formula $Ca_3(Fe_{0.85},Al_{0.15})_2Si_{1.15}O_{4.6}(OH)_{7.4}$ was used for the refinement. Even though at ambient conditions siliceous hydrogarnets tend to be poorly crystalline or possess a very small crystal size (as reported by [18]) resulting in extremely broad reflections, the Rietveld analysis (Table 5) clearly revealed that in the converter slag system hydrogarnet is the main crystalline hydration product. The amount of the hydrogarnet formed correlates well with the extent of the brownmillerite hydration, increasing with the increased dosage of tri-potassium citrate. The SEM image presented in Fig. 6 provides an indication of the morphology of hydrogarnet crystals in the BOF slag paste [39,40].

The formation of pyroaurite and portlandite is also observed in the XRD patterns. Pyroaurite, as a Fe-rich member of the hydrotalcite group (pyroaurite $Mg_6Fe^{3+}_2(OH)_{16}[CO_3]\cdot 4H_2O$) gives a broad reflection at around $2\theta = 13.5°$ whereas the strongest reflection of portlandite is located at $2\theta = 21.1°$. The content of portlandite in the hydrated samples is reduced with the addition of a tri-potassium citrate activator.

The presence of hydrogarnet and other hydration products in BOF slag pastes was further confirmed with the TG-DTG method, as shown in Fig. 7. Mass loss observed in the temperature range between 200 °C and 400 °C can be assigned to the water loss from siliceous hydrogarnet [18]. In agreement with the XRD Rietveld results, the formation of siliceous hydrogarnet occurs mostly within 7 days of hydration, and its extent is greater for higher dosages of tri-potassium citrate. In this temperature range, the decomposition of pyroaurite also takes place [41]. Rozov et al. [42] reported that pyroaurite decomposes at slightly lower temperatures than Al-rich hydrotalcite; however, it follows the same sequence of steps, comprising the loss of interlayer water, the decomposition of hydroxyl groups and decomposition of carbonate anions. With the DTG method, the presence of amorphous C-S-H gel could also be identified with the main mass loss due to the water release below 200 °C. The amount of C-S-H gel formed after 7 days of hydration differs substantially between the samples, being higher for the samples with a higher activator dosage, whereas after 28 days it is similar for all samples. This observation agrees with the rate and extent of belite hydration, as measured with the XRD Rietveld method. It can be therefore

Table 5
The phase composition of the hydrated BOF slag pastes in comparison to unhydrated slag in wt%, determined by XRD-Rietveld analysis.

Phase	BOF	7 days				28 days				*St. dev.
		C0	C1	C2	C3	C0	C1	C2	C3	
Wuestite	21.1	19.5	19.4	17.9	15.3	18.4	15.9	16.5	15.9	*1.1*
Magnetite	10.9	11.2	11.3	11.0	11.5	11.3	10.8	10.9	11.1	*0.8*
C_2S (α' + β)	31.8	30.2	28.8	28.7	27.3	26.0	22.2	25.3	27.4	*1.9*
Brownmillerite	17.4	17.2	11.1	8.1	6.3	14.3	10.8	7.8	6.6	*0.9*
Hydrogarnet	0.0	5.3	10.8	13.3	15.1	8.7	14.0	15.0	16.2	
Portlandite	1.2	1.2 (1.7)	0.5 (0.8)	0.5 (0.4)	0.3 (0.5)	1.5 (2.0)	0.7 (1.3)	0.5 (1.1)	0.4 (0.9)	*0.2*
Lime	0.5	0.5	0.4	0.4	0.4	0.3	0.4	0.3	0.3	*0.1*
Calcite	0.6	0.2	0.2	0.2	0.1	0.5	0.3	0.3	0.2	*0.1*
Amorphous**	16.5	18.7	23.6	29.2	35.0	26.0	33.6	33.7	34.2	*4.5*

() amount of portlandite determined with thermogravimetric analysis (tangential method)
* Standard deviations are derived from 3 independent measurements of unhydrated BOF slag.
** Pyroaurite is included in the amorphous phase due to its low content in hydration products and low crystallinity.

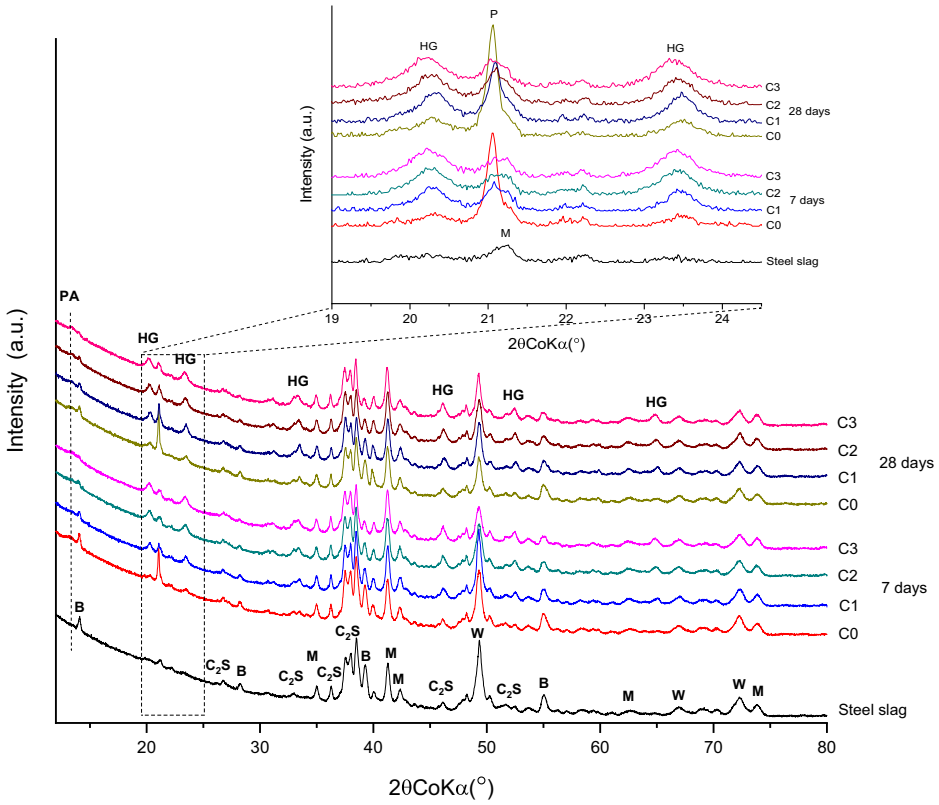

Fig. 5. XRD patterns of BOF slag and hydrated pastes (Legend: B-Brownmillerite, C_2S-Belite, M-Magnetite, W-Wuestite, P-Portlandite, HG-Hydrogarnet, PA-Pyroaurite).

concluded that in BOF slag systems, brownmillerite hydrates (in the presence of C_2S) to form mainly siliceous hydrogarnet whereas hydration of C_2S leads mainly to the formation of C-S-H gel.

It is not clear whether in the presented systems C-S-H gel can uptake Fe^{3+}. The formation of the C-S-H next to hydroandradite was found to be unavoidable even during the synthesis of siliceous hydrogarnet [17]. Whereas Labhasetwar [43] suggested the possibility of Fe^{3+} inclusion in the C-S-H gel, from the thermodynamic calculations it appears that in the hydrated Portland cement, iron is mostly present in the siliceous hydrogarnet [18]. As in our study alkalinizing additive was used, the behavior of Fe^{3+} species similar as in alkali-activated systems should also be considered. Daux et al. [44] showed that in alkali-activated systems after the dissolution of iron-rich precursor precipitation of Fe is much faster than precipitation of Si and Al. Fe^{3+} is found to act similarly as Ca^{2+}, removing OH- groups due to the precipitation of hydroxides and oxyhydroxides [45]. In the same time, an indication of Al^{3+} substitution with Fe^{3+} in the aluminosilicate structure was also reported [46]. For aluminum deficient systems like LD-slag, however, no data is available.

Besides C-S-H gel and hydroandradite/pyroaurite, the mass losses due to portlandite decomposition at around 430 °C and decomposition of carbonates/citrate compounds between 600 and 800 °C are observed. The amount of portlandite decreases when higher activator dosages are applied, which correlates well with the XRD results.

The mass loss in the temperature range between 600 and 800 °C is intensified with the increasing content of tri-potassium citrate. In this range, decomposition of carbonates usually takes place. It should be emphasized, however, that special care was taken during the sample curing and hydration stoppage to avoid the carbonation. The samples were prepared and measured twice, leading to the same results. It is therefore proposed that citrate compounds were formed and contributed to the mass change in this temperature range. As no crystalline citrate

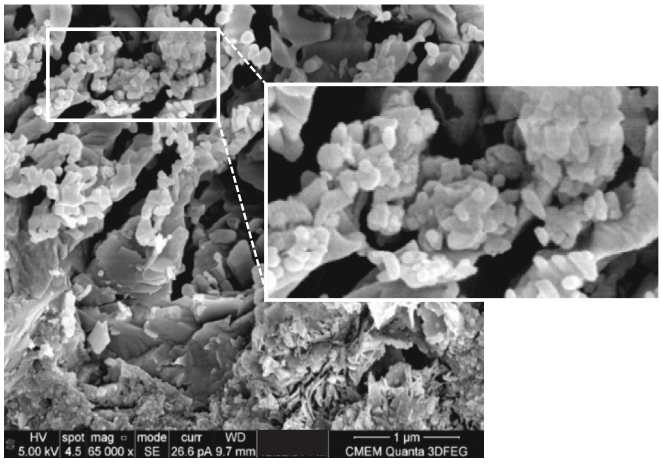

Fig. 6. BOF slag paste hydrated with 3 wt% of tri-potassium citrate for 28 days. Applied zoom indicates the location of hydrogarnet crystals.

precipitates could be identified with the XRD method, it is difficult to conclude in which form citrates are present in the system. From the FTIR measurements (Fig. 8) performed on the 28 days hydrated converter slag pastes, it is clear, however, that citrate groups remain in the samples after the hydration stoppage. Therefore, their presence in the pore solution is minimal or can be excluded since with the solvent exchange method, citrate ions would be removed with the pore solution. The infrared peaks located at 1569 and 1390 cm^{-1} are associated with the $\upsilon C{=}O$ and $\upsilon_{as}COO$ bands, respectively [25].

In order to determine the chemical composition of the hydration products, the PARC software was used. Fig. 9 shows an example of phase identification in the sample activated with 1 wt% of tri-potassium citrate after 28 days of curing.

In the PARC analysis, the individual phases of the hydration products could not be established due to the small crystal size of hydroandradite that is very well intermixed with C-S-H gel. Nevertheless, the averaged ratios of certain elements within the hydration products can be used to describe the differences between the chemical compositions of the products in the samples hydrated with varying dosages of tri-potassium citrate. Fig. 10 shows the molar ratios of Al/Si and V/Si vs. Ca/Si ratio. The results correspond well with the findings described with the Rietveld analysis. With increasing tri-potassium citrate dosage, Al/Si ratio and Ca/Si ratio (Fig. 10 a)) proportionally increase, confirming the enhanced reactivity of the brownmillerite in the presence of activator (as brownmillerite is the only source of aluminum). Since brownmillerite is highly contaminated with vanadium (see Table 4), vanadium content in the hydration products was also investigated. As shown in Fig. 10 b) for vanadium, a similar trend was observed as for aluminum, showing that vanadium was not removed from the sample during the hydration stoppage procedure, which indicates that it is most likely immobilized within the hydration products.

3.5. Microstructure and mechanical properties

Given that the addition of tri-potassium citrate considerably reduces the water demand of the slag pastes, low porosity and high mechanical performance were expected for the activated samples. The MIP results of the slag pastes after 28 days of hydration are shown in Fig. 11. A higher water requirement of the reference sample in order to obtain a similar consistency of all investigated pastes resulted in high porosity, as presented in Fig. 11 and, in consequence, low mechanical performance ~19 MPa at 28 days (Fig. 12). For the potassium citrate activated samples, the capillary porosity is strongly reduced, and the cumulative porosity decreases with the increased amount of activator, which is in agreement with the higher amounts of hydration products observed with the thermogravimetric method and XRD Rietveld analysis.

The changes in the porosity, however, do not reflect the changes in mechanical performance. Whereas at 7 days of hydration, the

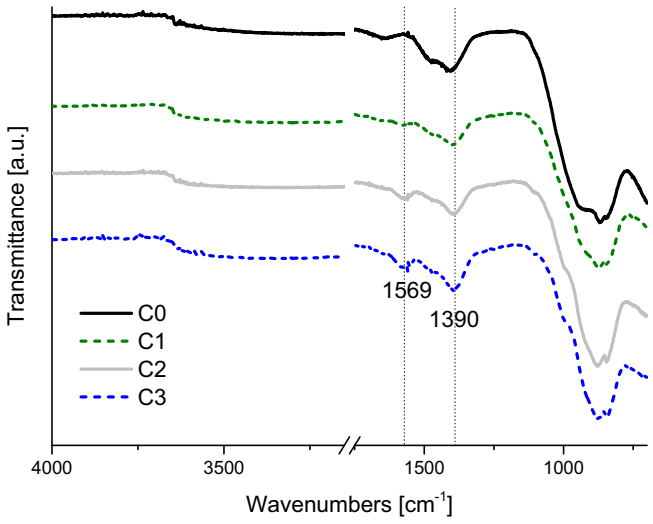

Fig. 8. FTIR spectra of converter slag pastes after 28 days of hydration.

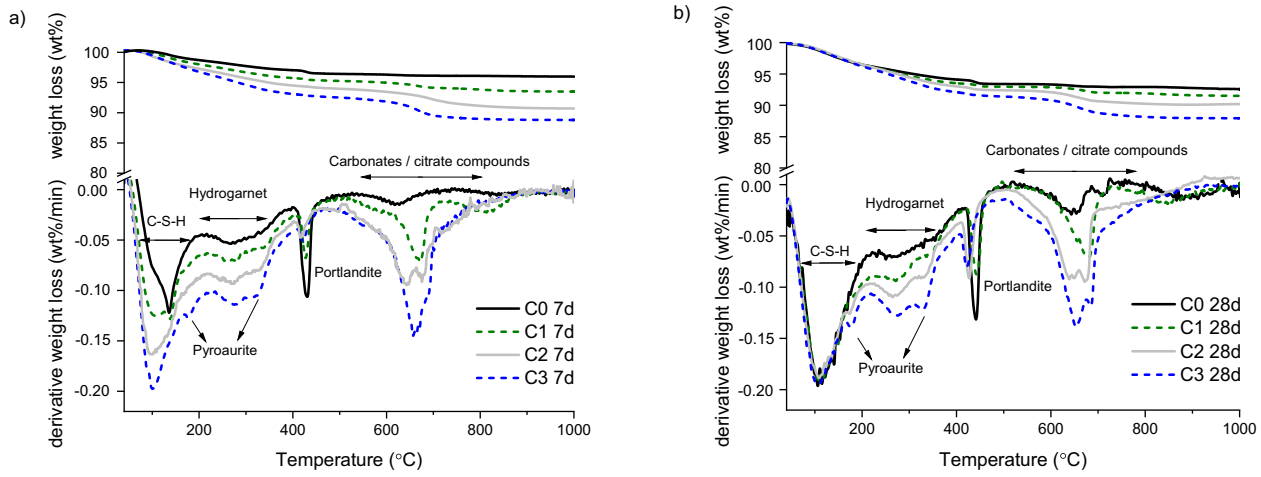

Fig. 7. Thermal analysis (TG and DTG) of slag pastes with dosages of tri-potassium citrate varying from 0 to 3 wt% after 7 and 28 days of hydration.

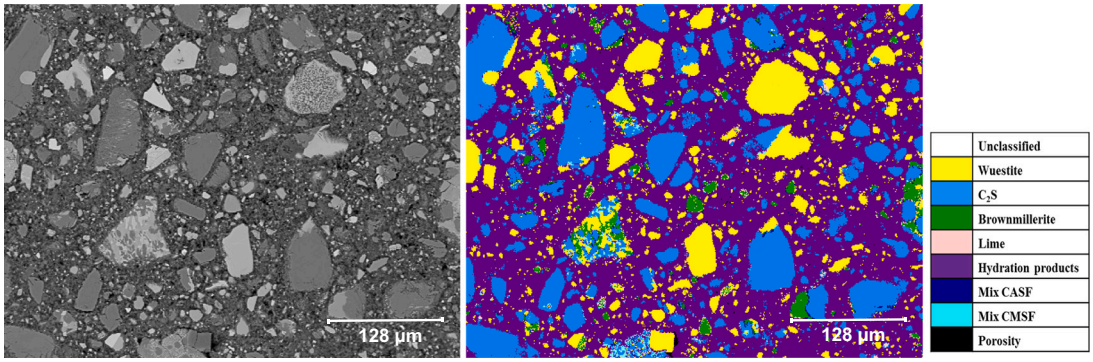

Fig. 9. Representative BSE image of hydrated slag paste with tri-potassium citrate dosage of 1 wt%.

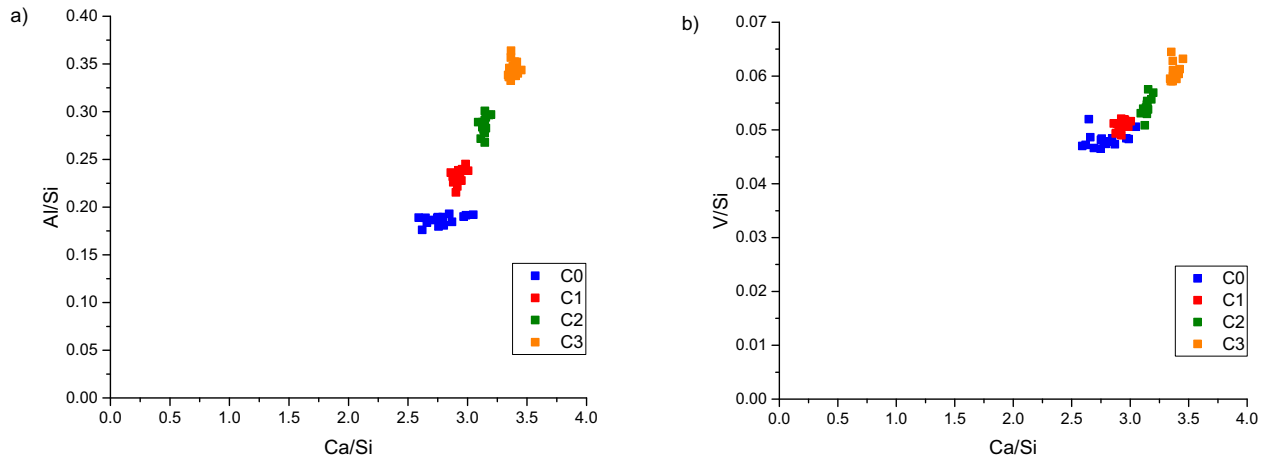

Fig. 10. Molar ratios a) Al/Si vs. Ca/Si and b) V/Si vs. Ca/Si of the hydration products in the samples with varying dosages of tri-potassium citrate (0 to 3 wt%), hydrated for 28 days (each dot represents averaged EDX data from the SI field of 512 × 384 pixels).

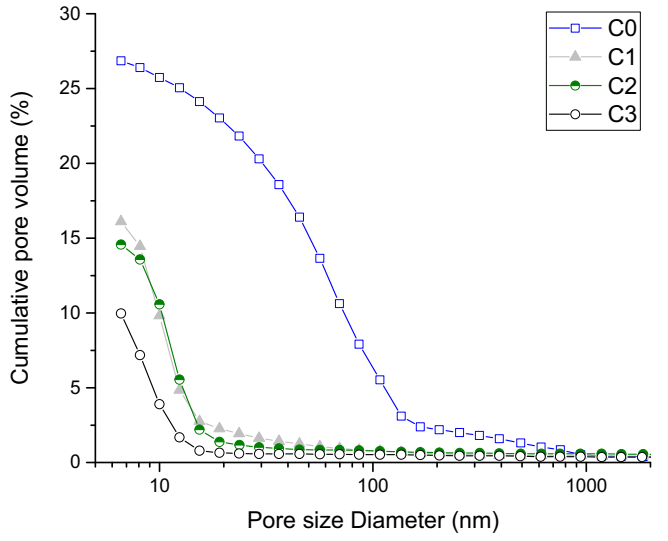

Fig. 11. The cumulative pore volume of converter slag pastes after 28 days of hydration.

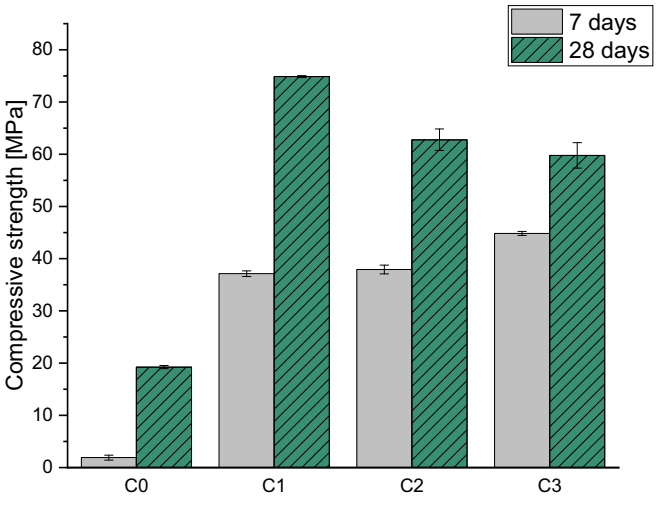

Fig. 12. Compressive strength of the converter slag pastes with dosages of tri-potassium citrate varying from 0 to 3 wt% after 7 and 28 days of hydration.

mechanical performance is improved with the increased activator dosage, at 28 days the optimum dosage of potassium citrate is equal to 1 wt%, resulting in compressive strength of 75 MPa. Further increase of activator amount results in the decrease of compressive strength to 63 MPa and 60 MPa for activator dosage of 2 wt% and 3 wt%, respectively.

From Fig. 13, showing the potassium distribution in the hydrated paste, it is clear that cracks have been formed in the areas highly enriched in potassium. It is therefore postulated that the decrease of the compressive strength observed for the pastes with the increasing activator dosage is a result of the incompatibility of C-S-H gel and the potassium-enriched gel. The presence of cracks in alkali-activated

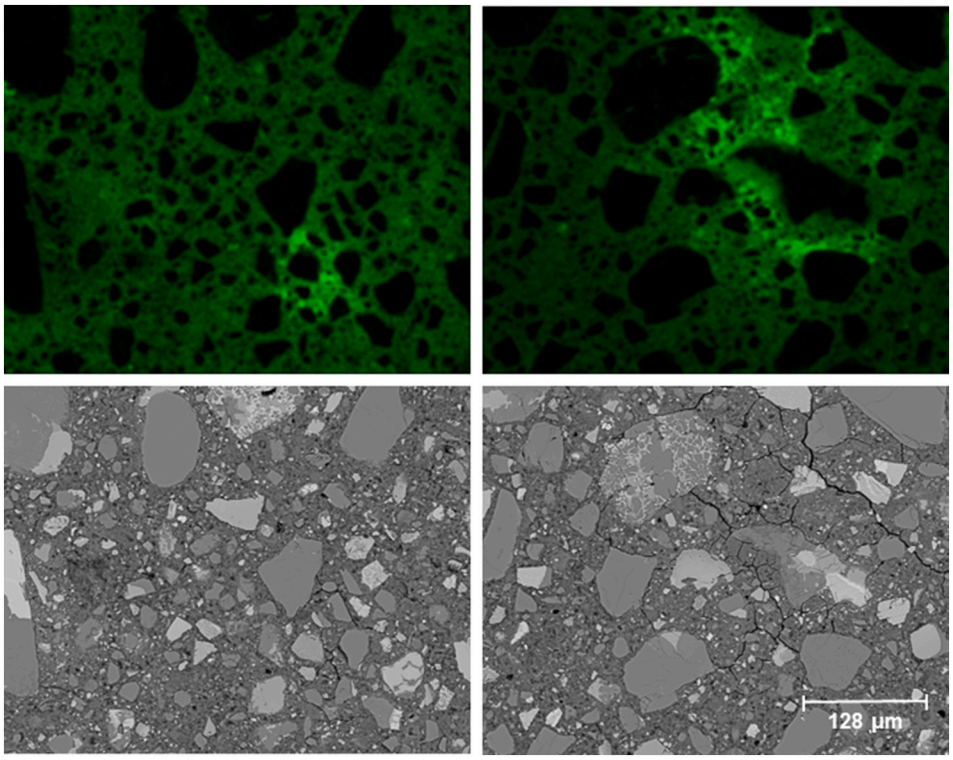

Fig. 13. Potassium distribution (derived from EDX mapping analysis) in the hydrated slag paste (C3) and the corresponding grey-scale image of the investigated area.

materials can be caused by the reorganization of the alkali products to form a denser gel, autogenous shrinkage, or the differences in the kinetics of the formation of the gels [47–49]. Furthermore, the slightly higher extent of belite hydration in the sample with 1 wt% of potassium citrate, as revealed with Rietveld XRD method, is an additional factor contributing to the improved strength of this sample.

3.6. Environmental impact

The BOF slag used in this study contains chromium (Cr) and vanadium (V) (see Table 1). As shown in Table 4, Cr and V are mostly incorporated in the reactive slag phases (belite and brownmillerite), implying a potential risk of leaching of those elements during the service life of BOF slag based materials.

The Dutch Soil Quality Decree (SQD) [31] specifies the limit values for leaching of environmentally sensitive elements from the materials in civil applications. In this study, the one batch leaching test was performed in order to evaluate the environmental impact of the raw material as well as the paste samples after 28 days of hydration. The results are shown in Table 6. For non-treated BOF slag, high leaching of vanadium is observed, exceeding twice the limit value specified in the SQD legislation, which is commonly reported for BOF slag [2]. Similarly, the leaching of chromium, second most abundant heavy metal in slag, is detected, however, falls below the limit level. The leaching of heavy metals from all the 28-days BOF slag pastes is very limited.

The minor leaching values of Cr and V from the converter slag pastes together with the high contents of vanadium in the reaction products, as shown in the Fig. 10b), clearly show that heavy metals are very well retained within the hydrated slag structure. From the literature it appears that C-S-H gel can immobilize Cr, whereas immobilization of V in the C-S-H phase remains questionable [50–52]. Hydroandradite $A_3B_2(SiO_4)_{3-x}(OH)_{4x}$ (as member of hydrogarnet family) also possesses a high capacity to immobilize heavy metals. The Cr^{3+} and V^{3+} can occupy the B site in hydroandradite, substituting trivalent cations (Fe^{3+} and Al^{3+}). At higher oxidations states chromium and vanadium can potentially substitute the hydroxyls ($H_4O_4^{4-}$) in the form of oxyanions (CrO_4^{2-}, VO_4^{3-}). The immobilization of heavy metals in hydrogarnets has also been observed in previous studies [39,53,54]. Nonetheless, when samples are exposed to CO_2, the drop of pH can lead to an increased release of vanadium [2]. Therefore, further investigation is required in order to evaluate the influence of the materials aging and the neutralization effects on the retention of contaminants in the BOF slag hydration products.

Table 6
Leaching of inorganic contaminants measured by one stage batch leaching test and the SQD limit values.

Parameter	Unshaped material (SQD)	BOF slag	C0	C1	C2	C3
	mg/kg	mg/kg	mg/kg	mg/kg	mg/kg	mg/kg
Antimony (Sb)	0.32	bdl[a]	0.16	0.15	0.17	0.15
Arsenic (As)	0.90	0.02	0.10	0.12	0.10	0.10
Cadmium (Cd)	0.04	bdl	bdl	bdl	bdl	bdl
Chromium (Cr)	0.63	0.28	0.03	0.05	0.01	0.03
Cobalt (Co)	0.54	bdl	bdl	bdl	bdl	bdl
Coper (Cu)	0.90	bdl	bdl	bdl	bdl	bdl
Lead (Pb)	2.30	bdl	bdl	bdl	bdl	bdl
Molybdenum (Mo)	1.00	0.02	bdl	bdl	bdl	bdl
Nickel (Ni)	0.44	bdl	bdl	bdl	bdl	bdl
Tin (Sn)	0.40	bdl	bdl	bdl	bdl	bdl
Vanadium (V)	1.80	3.78	0.10	0.13	0.09	0.18
Zinc (Zn)	4.50	bdl	0.12	0.11	0.13	0.13

[a] bdl-below detection limit.

4. Conclusions

This work presents a novel concept to utilize BOF slag as a high-performance cementitious binder in the concrete industry. With the

aim to activate iron-containing phases, a tri-potassium citrate monohydrate additive was applied to produce slag pastes, and the optimum dosage was evaluated. One additive-free sample was also prepared for comparison. The experimental investigation leads to the following conclusions:

- K_3-citrate promotes the dissolution and hydration of brownmillerite phase. The majority of brownmillerite is hydrated within 24 h, and the reaction rate is controlled by the activator dosage. The degree of brownmillerite hydration after 28 days increases with the increasing activator dosage.
- In the presence of activator, hydration of belite and wuestite is accelerated at the early ages. The extent of belite hydration after 28 days shows its maximum in this study with the addition of 1 wt% of potassium citrate.
- The main reaction products of BOF slag hydration are hydroandradite, pyroaurite, and C-S-H gel. Most likely, their high capacity to immobilize heavy metals prevents the leaching of chromium and vanadium from 28 days hydrated pastes.
- The addition of K_3-citrate significantly reduces the water demand of slag pastes. The superplasticizing function of tri-potassium citrate additive is crucial, enabling the production of converter slag pastes with low porosity (between 10 and 16%, depending on the activator dosage) and high compressive strength up to 75 MPa after 28 days of hydration.

CRediT authorship contribution statement

A.M. Kaja: Conceptualization; Methodology; Investigation; Data curation; Formal analysis; writing-original draft

K. Schollbach: Writing – Review Editing

S. Melzer: Writing – Review Editing

S.R. van der Laan: Writing – Review Editing

H.J.H. Brouwers: Funding acquisition; Supervision, Writing – Review Editing

Qingliang Yu: Conceptualization; Funding acquisition; Supervision, Writing – Review Editing

Declaration of competing interest

The authors declare that they have no known competing financial interests or personal relationships that could have appeared to influence the work reported in this paper.

Acknowledgment

The authors would like to acknowledge the financial support by NWO (The Netherlands Organisation for Scientific Research) for funding this research (project no. 12824). Special thanks are given to Corrie van Hoek for her help with PARC measurements.

References

[1] C. Shi, Characteristics and cementitious properties of ladle slag fines from steel production, Cem. Concr. Res. 32 (3) (2002) 459–462.
[2] A. van Zomeren, S.R. van der Laan, H.B.A. Kobesen, W.J.J. Huijgen, R.N. J. Comans, Changes in mineralogical and leaching properties of converter steel slag resulting from accelerated carbonation at low CO2pressure, Waste Manag. 31 (11) (2011) 2236–2244.
[3] S.Y. Pan, R. Adhikari, Y.H. Chen, P. Li, P.C. Chiang, Integrated and innovative steel slag utilization for iron reclamation, green material production and CO2fixation via accelerated carbonation, J. Clean. Prod. 137 (2016) 617–631.
[4] S. Z. Carvalho, F. Vernilli, B. Almeida, M. Demarco, and S. N. Silva, "The recycling effect of BOF slag in the portland cement properties," *Resour. Conserv. Recycl.*, vol. 127, no. September, pp. 216–220, 2017.
[5] "Euroslag," 2016. [Online]. Available: http://www.euroslag.com/products/statistics/2016/. [Accessed July 19, 2018].
[6] D. Wang, J. Chang, and W. S. Ansari, "The effects of carbonation and hydration on the mineralogy and microstructure of basic oxygen furnace slag products," *J. CO2 Util.*, vol. 34, pp. 87–98, Dec. 2019.
[7] F. Han, Z. Zhang, Properties of 5-year-old concrete containing steel slag powder, Powder Technol. 334 (2018) 27–35.
[8] J. Li, Q. Yu, J. Wei, T. Zhang, Structural characteristics and hydration kinetics of modified steel slag, Cem. Concr. Res. 41 (3) (2011) 324–329.
[9] F. Han, Z. Zhang, D. Wang, P. Yan, Hydration heat evolution and kinetics of blended cement containing steel slag at different temperatures, Thermochim. Acta 605 (2015) 43–51.
[10] Y. Jiang, T. C. Ling, C. Shi, and S. Y. Pan, "Characteristics of steel slags and their use in cement and concrete—A review," *Resour. Conserv. Recycl.*, vol. 136, no. December 2017, pp. 187–197, 2018.
[11] B. Das, S. Prakash, P.S.R. Reddy, V.N. Misra, An overview of utilization of slag and sludge from steel industries, Resour. Conserv. Recycl. 50 (1) (2007) 40–57.
[12] L. De Windt, P. Chaurand, J. Rose, Kinetics of steel slag leaching: batch tests and modeling, Waste Manag. 31 (2) (2011) 225–235.
[13] E. Belhadj, C. Diliberto, A. Lecomte, Characterization and activation of basic oxygen furnace slag, Cem. Concr. Compos. 34 (1) (2012) 34–40.
[14] Q. Wang, J.W. Yang, P.Y. Yan, Influence of initial alkalinity on the hydration of steel slag, Sci. China Technol. Sci. 55 (12) (2012) 3378–3387.
[15] S. Kourounis, S. Tsivilis, P.E. Tsakiridis, G.D. Papadimitriou, Z. Tsibouki, Properties and hydration of blended cements with steelmaking slag, Cem. Concr. Res. 37 (6) (2007) 815–822.
[16] Y.M. Kim, S.H. Hong, Influence of minor ions on the stability and hydration rates of β-dicalcium silicate, J. Am. Ceram. Soc. 87 (5) (2004) 900–905.
[17] B.Z. Dilnesa, E. Wieland, B. Lothenbach, R. Dähn, K.L. Scrivener, Fe-containing phases in hydrated cements, Cem. Concr. Res. 58 (2014) 45–55.
[18] B.Z. Dilnesa, B. Lothenbach, G. Renaudin, A. Wichser, D. Kulik, Synthesis and characterization of hydrogarnet Ca3(AlxFe1 - X)2(SiO4)y(OH)4(3 - y), Cem. Concr. Res. 59 (2014) 96–111.
[19] K.L. Scrivener, T. Füllmann, E. Gallucci, G. Walenta, E. Bermejo, Quantitative study of Portland cement hydration by X-ray diffraction/Rietveld analysis and independent methods, Cem. Concr. Res. 34 (9) (Sep. 2004) 1541–1547.
[20] F. Bullerjahn, M. Ben Haha, and K. L. Scrivener, "Iron solid solutions of ye ' elimite - Effect on reactivity," *19. Int. Baustofftagung ibausil*, no. October, 2015.
[21] W. Kurdowski, *Cement and Concrete Chemistry*. .
[22] W. Schwarz, Novel cement matrices by accelerated hydration of the ferrite phase in portland cement via chemical activation: kinetics and cementitious properties, Adv. Cem. Based Mater. 2 (5) (1995) 189–200.
[23] W. Stumm, Chemistry of the Solid-Water Interface, John Wiley & Sons, Inc., 1992.
[24] G. Möschner, B. Lothenbach, R. Figi, R. Kretzschmar, Influence of citric acid on the hydration of Portland cement, Cem. Concr. Res. 39 (4) (2009) 275–282.
[25] M.E. Ramos, F.J. Huertas, Adsorption of lactate and citrate on montmorillonite in aqueous solutions, Appl. Clay Sci. 90 (2014) 27–34.
[26] B. Mota, T. Matschei, and K. Scrivener, "Impact of NaOH and Na2SO4 on the kinetics and microstructural development of white cement hydration," *Cem. Concr. Res.*, vol. 108, no. February, pp. 172–185, 2018.
[27] C. van Hoek, J. Small, S. van der Laan, Large-area phase mapping using PhAse Recognition and Characterization (PARC) software, Micros. Today 24 (05) (2016) 12–21.
[28] D. Jansen, F. Goetz-Neunhoeffer, C. Stabler, J. Neubauer, A remastered external standard method applied to the quantification of early OPC hydration, Cem. Concr. Res. 41 (6) (2011) 602–608.
[29] D. Jansen, C. Stabler, F. Goetz-Neunhoeffer, S. Dittrich, J. Neubauer, Does ordinary Portland cement contain amorphous phase? A quantitative study using an external standard method, Powder Diffract. 26 (01) (2011) 31–38.
[30] A. C. A. Muller and K. L. Scrivener, "A reassessment of mercury intrusion porosimetry by comparison with1H NMR relaxometry," *Cem. Concr. Res.*, vol. 100, no. April, pp. 350–360, 2017.
[31] "Soil Quality Decree," 2015. [Online]. Available: http://wetten.overheid.nl/BWBR0023085/2015-07-01#BijlageA. [Accessed July 19, 2018].
[32] J.T. Pacanovsky, L. Huang, T. Frank, M. Samy, Hydration Control of Cementitious Systems, 1996.
[33] I. Strandkvist, Å. Sandström, F. Engström, Effect of FeO/MgO ratio on dissolution and leaching of magnesiowüstite, Steel Res. Int. 88 (6) (2017) 1–7.
[34] G.R. Qian, D.D. Sun, J.H. Tay, Z.Y. Lai, Hydrothermal reaction and autoclave stability of Mg bearing RO phase in steel slag, Br. Ceram. Trans. 101 (4) (2002) 159–164.
[35] R.S. Gollop, H.F.W. Taylor, Microstructural and microanalytical studies of sulfate attack. II. Sulfate-resisting Portland cement: ferrite composition and hydration chemistry, Cem. Concr. Res. 24 (7) (1994) 1347–1358.
[36] B. Lothenbach, E. Wieland, A thermodynamic approach to the hydration of sulphate-resisting Portland cement, Waste Manag. 26 (7) (2006) 706–719.
[37] H.F.W. Taylor, D.E. Newbury, An electron microprobe study of a mature cement paste, Cem. Concr. Res. 14 (4) (1984) 565–573.
[38] V. Morin, P. Termkhajornkit, B. Huet, and G. Pham, "Impact of quantity of anhydrite, water to binder ratio, fineness on kinetics and phase assemblage of belite-ye'elimite-ferrite cement," *Cem. Concr. Res.*, vol. 99, no. December 2015, pp. 8–17, 2017.
[39] S. Hillier, D.G. Lumsdon, R. Brydson, E. Paterson, Hydrogarnet: a host phase for Cr (VI) in chromite ore processing residue (COPR) and other high pH wastes, Environ. Sci. Technol. 41 (6) (2007) 1921–1927.
[40] S. Fujita, K. Suzuki, Y. Shibasaki, T. Mori, Synthesis of hydrogarnet from molten slag and its hydrogen chloride fixation performance at high temperature, J. Mater. Cycles Waste Manag. 4 (1) (2002) 70–76.
[41] M. Zajac, S.K. Bremseth, M. Whitehead, M. Ben Haha, Effect of CaMg(CO3)2 on hydrate assemblages and mechanical properties of hydrated cement pastes at 40 °C and 60 °C, Cem. Concr. Res. 65 (2014) 21–29.

[42] K. Rozov, et al., Synthesis and characterization of the LDH hydrotalcite-pyroaurite solid-solution series, Cem. Concr. Res. 40 (8) (2010) 1248–1254.
[43] N. K. Labhasetwar, "Miissbauer Study on Iron-exchanged Calcium Silicate Hydrate" vol. 87, pp. 82–87, 1991.
[44] V. Daux, G. Christophe, T. Advocat, J.L. Crovisier, P. Stille, Kinetic aspects of basaltic glass dissolution at 90°c: role of aqueous silicon and aluminium, Chem. Geol. 142 (1–2) (1997) 109–126.
[45] J.S.J. van Deventer, J.L. Provis, P. Duxson, G.C. Lukey, Reaction mechanisms in the geopolymeric conversion of inorganic waste to useful products, J. Hazard. Mater. 139 (3) (2007) 506–513.
[46] N. Ye *et al.*, "Transformations of Na, Al, Si and Fe species in red mud during synthesis of one-part geopolymers," *Cem. Concr. Res.*, vol. 101, no. December 2016, pp. 123–130, 2017.
[47] A.M. Kaja, A. Lazaro, Q.L. Yu, Effects of Portland cement on activation mechanism of class F fly ash geopolymer cured under ambient conditions, Constr. Build. Mater. 189 (2018) 1113–1123.
[48] Y. Ma, G. Ye, The shrinkage of alkali activated fly ash, Cem. Concr. Res. 68 (2015) 75–82.
[49] I. García-Lodeiro, A. Fernández-Jiménez, A. Palomo, Variation in hybrid cements over time. Alkaline activation of fly ash-portland cement blends, Cem. Concr. Res. 52 (2013) 112–122.
[50] A. Polettini, R. Pomi, P. Sirini, Fractional factorial design to investigate the influence of heavy metals and anions on acid neutralization behavior of cement-based products, Environ. Sci. Technol. 36 (7) (2002) 1584–1591.
[51] A. Vollpracht, W. Brameshuber, Binding and leaching of trace elements in Portland cement pastes, Cem. Concr. Res. 79 (2016) 76–92.
[52] N.D.M. Evans, Binding mechanisms of radionuclides to cement, Cem. Concr. Res. 38 (4) (2008) 543–553.
[53] I. Moulin, J. Rose, W. Stone, and J. Bottero, "Lead, zinc and chromium (III) and (VI) speciation in hydrated cement phases," *Waste Mater. Constr.*, no. III, pp. 269–280, 2000.
[54] I.T. Burke, W.M. Mayes, C.L. Peacock, A.P. Brown, A.P. Jarvis, K. Gruiz, Speciation of arsenic, chromium, and vanadium in red mud samples from the Ajka spill site, Hungary, Environ. Sci. Technol. 46 (6) (2012) 3085–3092.